Thin Solid Films 582 (2015) 193–197

Contents lists available at ScienceDirect

Thin Solid Films

journal homepage: www.elsevier.com/locate/tsf

# Epitaxial $Cu_2ZnSnSe_4$ thin films and devices

Alex Redinger [a], Heiko Groiss [b], Jan Sendler [a], Rabie Djemour [a], David Regesch [a], Dagmar Gerthsen [b], Susanne Siebentritt [a,*]

[a] Laboratory for Photovoltaics, Physics and Materials Science Research Unit, University of Luxembourg, 41, rue du Brill, L-4422 Belvaux, Luxembourg
[b] Karlsruhe Institute of Technology, Laboratory for Electron Microscopy, Engesserstr. 7, D-76131 Karlsruhe, Germany

ARTICLE INFO

Available online 20 November 2014

*Keywords:*
Copper zinc tin selenide
Epitaxy
Kesterite
Transmission electron microscopy
Solar cells

ABSTRACT

Epitaxial $Cu_2ZnSnSe_4$ (CZTSe) thin films have been grown via high temperature coevaporation on GaAs(001). Electron backscattering diffraction confirms epitaxy in a wide compositional range. Different secondary phases are present in the epitaxial layer. The main secondary phases are $Cu_2SnSe_3$ and ZnSe which grow epitaxially on top of the CZTSe. Transmission electron microscopy measurements show that the epitaxial CZTSe grows predominantly parallel to the c-direction. Epitaxial CZTSe solar cells with a maximum power conversion efficiency of 2.1%, an open-circuit voltage of 223 mV and a current density of 16 mA/cm$^2$ are presented.



## 1. Introduction

The $Cu_2ZnSnSe_4$ (CZTSe) semiconductor compound is used as an absorber layer in thin film solar cells. The material exhibits a direct bandgap close to 1.0 eV and the current record power conversion efficiency is 9.7% [1]. One of the challenges of this material class is the theoretically predicted small single phase existence region [2], which was also measured experimentally [3]. The most prominent secondary phases are ZnSe and $Cu_2SnSe_3$ (CTSe). All three materials have very similar lattice constants and consequently they are very difficult to discriminate with conventional X-ray diffraction techniques. The solar cell absorbers are usually grown on molybdenum coated glass substrates. Consequently the absorbers are polycrystalline with typical grain sizes in the micrometre range. Secondary phases can been identified in most solar cell absorbers, at the heterojunction [4,5], at the back contact [6] and in the absorber layer [4]. Even in the current record sulfur–selenide devices with efficiencies up to 12.6% a ZnS(e) secondary phase is present at the heterojunction [7]. The secondary phases severely influence the optoelectronic properties of the absorbers and of the resulting devices.

The $Cu_2SnSe_3$ secondary phase is very harmful for the solar cells. The low bandgap material deteriorates the maximum open circuit voltage [8]. It has been shown recently that solar cells with a few nanometers of a $Cu_2SnSe_3$ on top of the CZTSe show no efficiency [4]. However, one has to be careful since CTSe can exist in different modifications. A monoclinic $Cu_2SnSe_3$ has been reported by Marcano et al. [9]. Moreover cubic $Cu_2SnSe_4$ [10], cubic $Cu_2SnSe_3$ [11] and a low temperature orthorhombic modification [12] have been reported.

The ZnSe secondary phase is not as harmful as the low bandgap CTSe. ZnSe is present in a lot of absorbers and has been reported to be responsible for current blocking [13], high series resistance [14] and increased reverse saturation current densities [4].

In polycrystalline absorbers the control and the detection of the secondary phases are very challenging. It is the aim of this contribution to shed light into the formation of the secondary phases in high temperature coevaporation. In order to simplify the situation CZTSe is grown epitaxially on GaAs(001) in order to form absorbers without grain boundaries and under well controlled conditions. The lattice mismatch of the substrate and the CZTSe film is only 0.6% and consequently epitaxial growth is possible.

## 2. Experimental

The absorber layers have been grown in a molecular beam epitaxy system equipped with four effusion cells (Zn, Cu, Sn, SnSe) and the selenium is supplied via a valved cracker source. The cracker of the source is heated to 1000 °C during deposition in order to maximize the reactivity of the selenium species. The GaAs(001) epi-ready wafers are heated to 500 °C prior to the deposition. The substrate temperature is monitored with a pyrometer. The growth process has already been described in [15] and consists of two stages. During the first stage, all five elements are coevaporared for a duration of 45 min. We used a Sn and a SnSe source in order to compensate for the SnSe losses during growth [16]. SnSe exhibits a significant vapour pressure at the growth temperature and consequently tin has to be supplied in excess. After 45 min the Cu and Zn sources are switched off and the absorber layer is annealed in a Sn, SnSe and Se atmosphere for additional 30 min. A similar post deposition annealing stage has also been described in [17] in the case of polycrystalline CZTSe growth. The film thicknesses of the absorbers presented in this manuscript are: 1.6 μm for the Cu-rich film, 1.1 μm for the stoichiometric film and slightly below 1 μm for the Zn-rich film.

* Corresponding author.
*E-mail address:* susanne.siebentritt@uni.lu (S. Siebentritt).

http://dx.doi.org/10.1016/j.tsf.2014.11.040
0040-6090/

The sample homogeneity has been analysed by scanning electron microscopy (SEM) equipped with an energy dispersive X-ray analysis (EDX) detector. The analysis presented in this study has been performed at 20 kV acceleration voltage. Epitaxy is confirmed via electron backscattering diffraction (EBSD) measured at 15 kV acceleration voltage with a beam current of 5 nA. The EBSD patterns presented here have been acquired by scanning the beam over an area of roughly 100 μm × 100 μm.

For transmission electron microscopy (TEM) investigations a Philips CM200 operated at 200 kV was used for electron diffraction and dark-field TEM experiments. The EDX measurements were performed with a TITAN³ 80-300 operated at 300 kV. The TEM cross-sectional specimens were prepared along the [110] crystallographic direction and $Ar^+$-ion milling was used for final thinning to electron transparency.

Micro-Raman spectroscopy has been performed in a home built confocal setup equipped with an argon ion laser operated at a laser wavelength of 514.5 nm.

Solar cells have been fabricated in a similar way as the CZTSe absorbers grown on Mo coated glass. After the absorber fabrication a CdS buffer layer is grown via chemical bath deposition followed by a magnetron sputtered undoped ZnO and Al-doped ZnO double layer. A Ni/Al grid is grown on top of the window layer and an Au back contact is grown at the back of the highly doped GaAs substrate. Consequently the film structure consists of n + window layer, a p-doped CZTSe and a p + GaAs substrate. In the case of $Cu(In,Ga)Se_2$, epitaxial solar cells with efficiencies close to 7% have been achieved with the same layer stacking [18].

## 3. Results

Fig. 1 depicts scanning electron microscopy images of the sample surfaces and electron backscattering diffraction images of corresponding samples. In Fig. 1(a), (d) the composition is Cu-rich and Zn-poor [Cu/(Zn + Sn) > 1, Zn/Sn < 1]. No grain boundaries are visible in the SEM micrograph and the large area EBSD analysis depicted in Fig. 1(d) corroborates that the sample is epitaxial. In the case of a polycrystalline sample no Kikuchi lines would be observed in the rastering mode over an area of 100 μm × 100 μm. An extremely large number of different Kikuchi lines would be superimposed and an EBSD pattern would be absent. As we observe clear Kikuchi lines which can be indexed with a single pattern, epitaxy is confirmed.

Lowering the Cu ratio leads to a significant roughening of the film and white patches with an extension of several micrometres are visible in the SEM micrograph (Fig. 1(b)). Despite the drastic change in morphology and the inhomogeneous appearance the sample is still epitaxial as shown in Fig. 1(e). Lowering the Cu ratio even further leads again to a more homogeneous film. The sample is epitaxial as shown in Fig. 1(f). The compositions of the films are all situated on the $Cu_2SnSe_3$/ZnSe tie line of the quasi ternary phase diagram, as already discussed in [15].

In all three cases the EBSD pattern has been acquired on a large area and only a single set of Kikuchi lines has been observed. The pattern has been indexed according to the I-42m crystal structure (ICDD: 04-010-6295) and good agreement has been achieved as shown in Fig. 2(a). It has to be noted here that the indexing shown in Fig. 2(a) has been done with the sample tilted by 70°. If the sample tilting is taken into account the out of plane orientation of the film is either (001) or (100). It was not possible to distinguish between the two possible growth directions of CZTSe. Moreover, we have to emphasize that we also found a good agreement if we consider a cubic zinc blende type structure. In CZTSe, the c/a ratio is very close to two and consequently the EBSD analysis is not capable of resolving the difference between a cubic ZnSe, a cubic/tetragonal CTSe or a tetragonal CZTSe crystal structure. Although the measurements confirm that the sample is epitaxial, we still observe a significant blurring of the EBSD pattern. The most likely reason is surface contamination which is known to reduce the EBSD signal [19]. The sample has been exposed to air several times for prolonged periods prior to the EBSD analysis. No cleaning of the surface has been done. Moreover, strain and mixtures of (001) and (100) oriented tetragonal and cubic phases will influence the pattern quality.

In order to analyse the inhomogeneous epitaxial absorbers further the samples have been analysed by Raman spectroscopy (Fig. 2(b)) and energy dispersive X-ray analysis as shown in Fig. 2(c)–(e). The Raman spectrum acquired on the Cu-rich film shows that the most intense Raman mode is located at 180 $cm^{-1}$. This mode is commonly attributed to a monoclinic $Cu_2SnSe_3$ [9]. However, all Raman peak positions have to be shifted by 3 $cm^{-1}$ to higher wavenumbers in order to

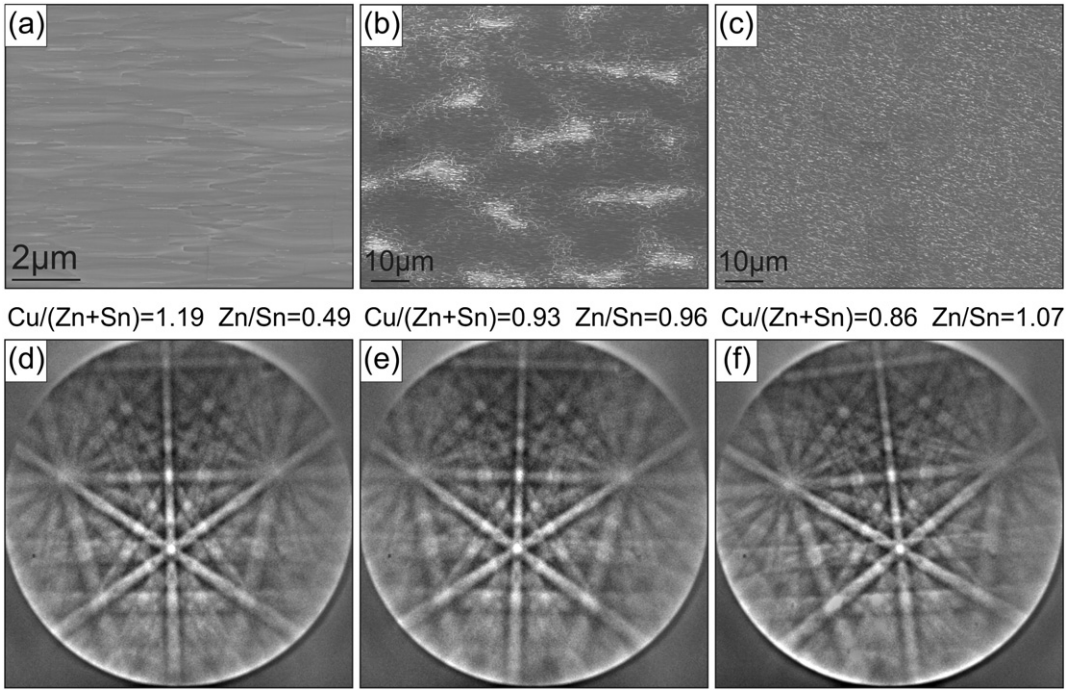


**Fig. 1.** SEM micrographs and corresponding large area EBSD patterns of three different samples with different compositions. (a), (d) Cu-rich and Sn-rich growth conditions, (b), (e) sample with a composition close to stoichiometry in the Zn/Sn ratio, (c), (f) Cu-poor and Zn-rich composition.

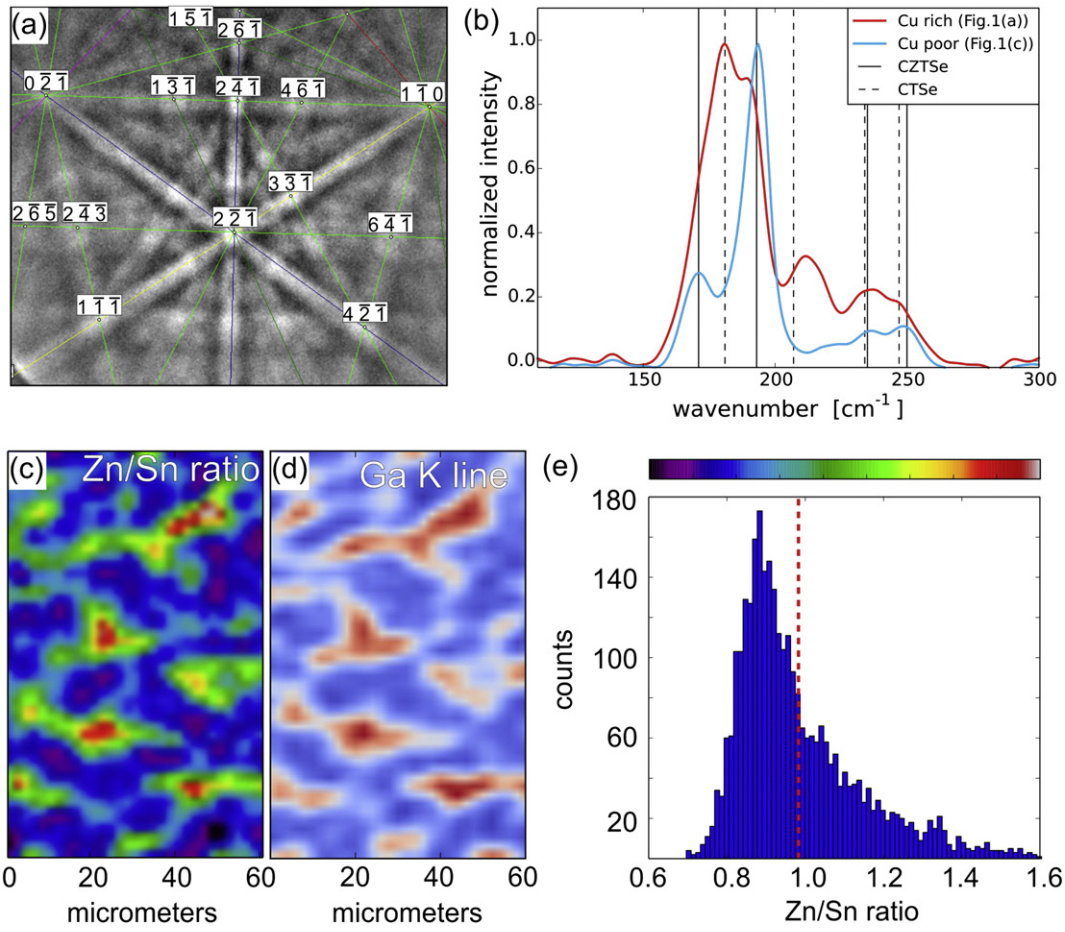


**Fig. 2.** (a) EBSD pattern indexed with the CZTSe pattern, (b) Raman spectra of the sample (a) and (c) in Fig. 1, (c), (d) EDX mapping acquired at 20 kV acceleration voltage. The Zn/Sn ratio is depicted in (c) and the Ga K line intensity is shown in (d). (e) The Zn/Sn ratios acquired during the mapping are plotted in a histogram. The ratio exhibits a long tail to high Zn/Sn ratios. The colour code above the graph is identical with the colour coding in Fig. 2(c).

fit the measurement. The other contributions in the Cu-rich film can be assigned to CZTSe where the two main modes are found at 193 $cm^{-1}$ and 171 $cm^{-1}$. It is interesting to note that the kesterite Raman modes are shifted by roughly 3 $cm^{-1}$ to lower wavenumbers. A possible explanation could be that the films are strained. However we did not yet perform further measurements to confirm this assumption. The stoichiometric and Zn-rich samples exhibit CZTSe Raman modes described in literature with two main modes at roughly 193 $cm^{-1}$ and 171 $cm^{-1}$ and two low intensity modes at 235 $cm^{-1}$ and 250 $cm^{-1}$. From the compositional point of view this result is nothing but expected. However, the EBSD patterns depicted in Fig. 1 are all very similar. A zoom in of Fig. 1(e) together with the indexing is depicted in Fig. 2(a). The indexing of the Kikuchi pattern is not compatible with the monoclinic CTSe fingerprint. From this analysis one has to conclude that there is no monoclinic CTSe phase present in the vicinity of the sample surface. This is particularly true for the Cu-rich sample where an additional Raman line at 180 $cm^{-1}$ in the near surface region is observed. This indicates that the Raman line at 180 $cm^{-1}$ does not originate from a monoclinic CTSe but rather from a cubic or tetragonal CTSe.

The stoichiometric sample presented in Fig. 1(b), (d) exhibits a very inhomogeneous surface. In order to analyse the sample further an EDX mapping has been performed and the result is shown in Fig. 2(c), (d). The composition at each measured position ($64 \times 48$ spots on roughly $130 \times 90\ \mu m^2$) has been deduced via a full EDX spectrum fitting including atomic number, absorption and fluorescence correction. This enables to get accurate element compositions and consequently also element ratios. The colour coded Zn/Sn ratio is shown in Fig. 2(c). The deduced ratios are also shown in a histogram presented in Fig. 2(e). The overall composition of the sample is close to stoichiometry. However some parts are Zn-rich and other parts are Zn-poor. The Zn-rich parts of the sample exhibit a much lower film thickness. This is shown in Fig. 2(d) where the Ga signal is shown as a function of position. We observe an excellent correlation of the Ga-signal with the Zn-rich parts of the sample. The Ga signal changes from 8 at.% (blue) to 24 at.% (red) in the case where the quantification is made with the following elements: Cu, Zn, Sn, Se, Ga, and As. The Zn-rich parts have been analysed with Raman spectroscopy with a laser excitation of 485 nm (data not shown) and we can confirm that a ZnSe secondary phase is present in these areas. However, we do not observe a complete phase segregation since in the Zn-rich areas a rather large Sn concentration is observed. We therefore conclude that a ZnSe secondary phase is present on top of the CZTSe. Due to the almost perfect lattice mismatch between ZnSe and CZTSe, the secondary phase grows epitaxially on top of the CZTSe.

The result is unexpected since the Zn-rich and Zn-poor areas are extremely large in dimension. The sample is grown via high temperature coevaporation. The element fluxes are homogeneously distributed on the atomic scale. Surface diffusion over tens of micrometres is a possible but unlikely explanation. Moreover, ZnSe and CZTSe are lattice matched and consequently both phases can coexist without the formation of a large number of dislocations, strain or grain boundaries. Lattice mismatch as the driving force for the phase segregation of ZnSe and CZTSe is not likely.

A plausible explanation could be that the growth rate depends on the orientation of the growing film and/or substrate termination. Different surfaces may form under Cu excess or Cu depletion which change

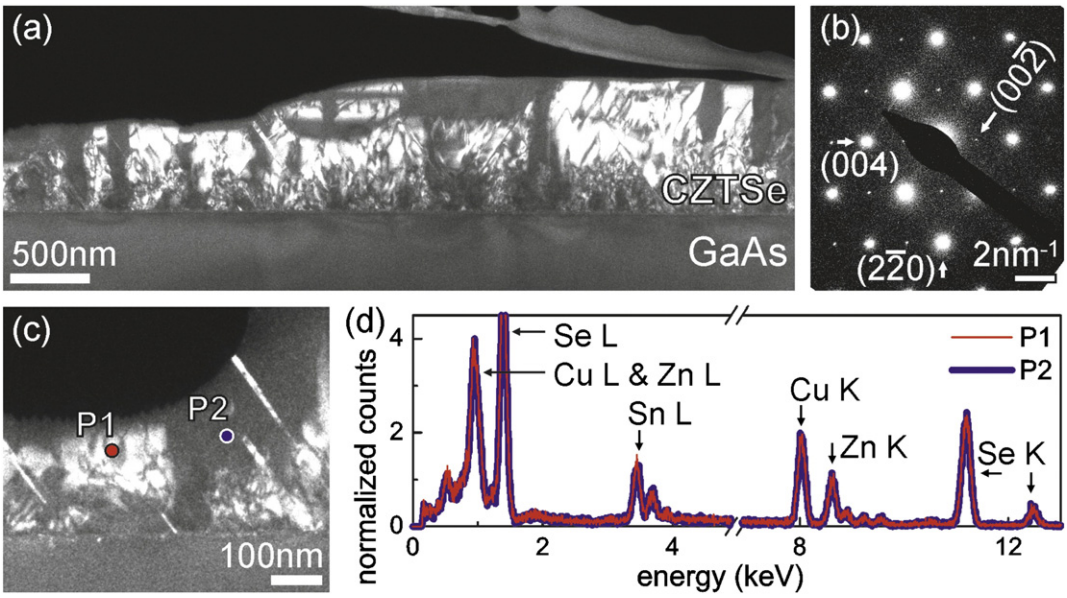


**Fig. 3.** (a) {002} DF TEM image of the sample depicted in Fig. 1(b). The diffraction pattern (b) depicts CZTSe along the [110] zone axis. Next to the (2$\bar{2}$0) and (004) reflections additional weak reflections are present. These reflections (e.g. marked (00$\bar{2}$) reflection) can be used to identify CZTSe with the c-axis parallel to the growth direction. (c) {002} DF TEM image with indicated EDX measuring points. (d) Comparison of two EDX spectra recorded at the positions marked in (c). Even if the crystal orientation at the two points is different, no differences can be seen in the spectra.

the sticking probabilities of the chalcogen and tin-chalcogenide. This phenomenon has also been observed in other material systems [20]. A direct consequence of different chalcogen sticking coefficients is the amount of decomposition which is well known in CZTSe [16]. However, more work has to be done in order to fully understand the growth of CZTSe and the interplay of CZTSe with the possible lattice matched ZnSe and CTSe.

In order to further investigate the epitaxial CZTSe films a TEM analysis was carried out and the results are presented in Fig. 3. Fig. 3(a) shows a dark-field (DF) TEM image of the CZTSe film depicted in Fig. 1(b). Similar results have been obtained for the sample presented in Fig. 1(a). The DF images were formed with the {002} reflections, which are only present for tetragonal (kesterite/stannite) CZTSe oriented along the [110] direction and a c-axis parallel to the growth direction (see Fig. 3(b)). To form the DF image the specimens were tilted to a so called two-beam condition, where the (002) reflection is excited with maximum intensity. Fig. 3(b) displays a diffraction pattern of CZTSe along the [110] zone axis. Indicated are the (004) and (2$\bar{2}$0) reflections, where the (004) reflection corresponds to the (002) reflection of a fcc material. The differences of the indices are a result of the factor two of the c/a ratio of the CZTSe unit cell compared to the cubic fcc unit cell. The cubic ZnSe, $Cu_2SnSe_3$ structures and tetragonal (kesterite/stannite) structure with c-axis parallel to the film/GaAs interface do not exhibit the additional weak reflections present in Fig. 3(b). Consequently this reflection can be used to unambiguously identify CZTSe with the c-axis parallel to the growth direction. In Fig. 3(a) we observe a mixture of bright and dark image intensities in the absorber layer. The first observation is that the majority of the film consists of CZTSe with the c-axis parallel to the growth direction, which corresponds to the bright regions of the image. The dark regions, which correspond to CZTSe with its c-axis aligned perpendicular to the growth direction or cubic ZnSe/CTSe, show a columnar morphology with columns extending from the interface to the top of the layer. However, there are also regions where the transition from bright to dark occurs in the middle of the absorber layer. The question immediately arises if the dark regions exhibit a different composition and if they are a secondary phase. Therefore the regions were analysed with EDX. In the DF image (Fig. 3(c)) two measuring positions P1 and P2 are marked, one in a bright, the other in a dark area of the film. In Fig. 3(d) one can see the overlay of the two EDX spectra. The spectra were normalized to adapt count number differences which originate from different sample thicknesses. Both spectra exhibit almost the same shape, no real differences can be seen in the peak height and shapes. This indicates similar composition at both positions and excludes secondary phases like ZnSe and CTSe.

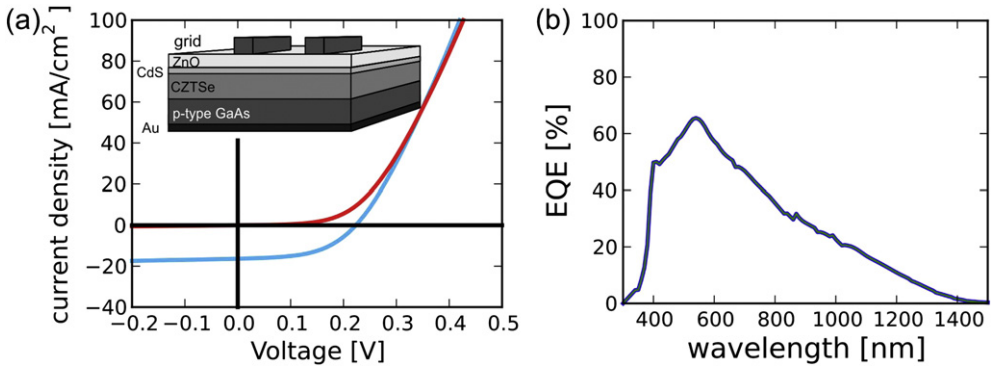


**Fig. 4.** (a) Current–voltage characteristics of the CZTSe solar cell. The inset schematically shows the stacking order of the solar cell device. (b) External quantum efficiency of the corresponding device.

Thus, this part of the sample consists of CZTSe and only the orientation of the c-axis varies. Quantitative analysis of the EDX yields for both points a composition of 23% Cu, 11% Zn, 17% Sn and 48% Se, which are compatible with the composition of CZTSe.

It has to be emphasized that the heterointerface is not abrupt and a large density of defects has been observed. This is certainly a direct consequence of the unoptimized surface preparation and an unsuitable surface termination of the GaAs prior the growth of CZTSe.

Solar cells have been fabricated with the procedure described in the experimental section and the results are presented in Fig. 4. The current–voltage characteristics are shown in Fig. 4(a) together with a sketch of the device structure and the external quantum efficiency is shown in Fig. 4(b). The solar cell absorber had a global composition of Cu / (Zn + Sn) = 0.86 and Zn/Sn ratio of 1.07. Solar cells produced from absorbers with a higher Sn content did not result in working devices. The best device exhibits an efficiency of 2.1% with a $V_{oc}$ = 223 mV, $J_{sc}$ = 18.2 mA/cm$^2$ and a fill factor of 51%. The quantum efficiency data depicted in Fig. 4(b) shows a maximum of only 65% and a very low response in the near IR region. On top of the absorber a large amount of ZnSe has been identified which is the likely reason for the low current density. ZnSe has been reported to strongly influence the current density due to current blocking [13]. Moreover a high Zn/Sn ratio is known to change the doping density of the absorbers [21]. The low IR response in the quantum efficiency measurement is probably a consequence of a very high doping and consequently a very small space charge region. Compared to the polycrystalline CZTSe record device, the open-circuit voltage only reaches a bit more than 50% of the polycrystalline value. It has to be emphasized at this point that no conclusion of the grain boundaries in CZTSe can be drawn from this solar cell result. Due to the unoptimized substrate cleaning extensive contaminations at the CZTSe/GaAs interface are present. In the film a large number of stacking faults, dislocations and (001)/(100) tetragonal CZTSe boundaries are present. The density of the crystallographic defects in the epitaxial films has to be reduced before a fair comparison between the epitaxial and the polycrystalline solar cells can be made. The result can also be interpreted differently. Even in CZTSe absorbers that are not single phase and where the density of the structural defects is enormously high the open circuit voltage already reaches more than half the value of the current polycrystalline record device. This actually shows that there is an extremely large potential for epitaxial CZTSe as absorbers in high efficiency thin film solar cells.

## 4. Summary

In summary, we have shown that CZTSe can be grown epitaxially on GaAs(001) by high temperature coevaporation in a broad compositional range. However, the Cu-rich films exhibit a $Cu_2SnSe_3$ secondary phase and the Cu-poor and Zn-rich films a ZnSe secondary phase. CZTSe, ZnSe and $Cu_2SnSe_3$ grow epitaxially on top and next to each other which makes their identification difficult. In the stoichiometric samples a very rough structure is formed with Zn-rich and Zn-poor regions. Transmission electron microscopy measurements show that CZTSe growths predominantly with the c-axis parallel to the growth direction. Until now no evidence of secondary phases within the CZTSe matrix has been found by TEM. However, there is a substantial amount of CZTSe with c-axis perpendicular to the growth direction present. We observe a high density of structural defects such as stacking faults and a large amount of contamination at the CZTSe/GaAs heterointerface. This is a direct consequence of the un-optimized GaAs surface preparation prior to the growth. Solar cells exhibit a power conversion efficiency up to 2.1%. It can be expected that the efficiency can be boosted significantly if the dislocation and stacking fault densities are decreased to an acceptable level.

## Acknowledgement

The authors acknowledge funding though the Luxembourgish FNR in the framework of the KITS2 project. H. Groiss acknowledges funding through the Austria Science Fund FWF, project number J3317-N27. J. Sendler acknowledges funding through the European initial training network programme Kestcells, project number FP7-PEOPLE-2012-ITN. 316488. We would like to acknowledge J. Schmauch at INM Saarbrücken for the EBSD measurements and useful discussions. The use of the SEM machine in the CRP-Gabriel Lippmann is acknowledged.

## References

[1] G. Brammertz, M. Buffière, S. Oueslati, H. ElAnzeery, K. Ben Messaoud, S. Sahayaraj, C. Köble, M. Meuris, J. Poortmans, Characterization of defects in 9.7% efficient $Cu_2ZnSnSe_4$–CdS–ZnO solar cells, Appl. Phys. Lett. 103 (16) (2013) 163904.
[2] A. Walsh, S. Chen, S.-H. Wei, X.-G. Go, Kesterite thin-film solar cells: advances in materials modelling of $Cu_2ZnSnS_4$, Adv. Energy Mater. 2 (2012) 400.
[3] I. Dudchak, L. Piskach, Phase equilibria in the $Cu_2SnSe_3$–$SnSe_2$–ZnSe system, J. Alloys Compd. 351 (2003) 145.
[4] M. Mousel, T. Schwarz, R. Djemour, T.P. Weiss, J. Sendler, J.C. Malaquias, A. Redinger, O. Cojocaru-Mirédin, P. Choi, S. Siebentritt, Cu-rich precursors improve kesterite solar cells, Adv. Energy Mater. 4 (2014) 1300543.
[5] W.-C. Hsu, I. Repins, C. Beall, C. DeHart, B. To, W. Yang, Y. Yang, R. Noufi, Growth mechanisms of co-evaporated kesterite: a comparison of Cu-rich and Zn-rich composition paths, Prog. Photovolt. Res. Appl. 22 (2012) 35.
[6] A. Redinger, K. Hönes, X. Fontané, V. Izquierdo-Roca, E. Saucedo, N. Valle, A. Pérez-Rodríguez, S. Siebentritt, Detection of a ZnSe secondary phase in coevaporated $Cu_2ZnSnSe_4$ thin films, Appl. Phys. Lett. 98 (2011) 101907.
[7] W. Wang, M.T. Winkler, O. Gunawan, T. Gokmen, T. Todorov, Y. Zhu, D.B. Mitzi, Device Characteristics of CZTSSe Thin-Film Solar Cells with 12.6% Efficiency, Adv. Energy Mater. 4 (2014) 1301465.
[8] S. Siebentritt, Why are kesterite solar cells not 20% efficient? Thin Solid Films 535 (2013) 1.
[9] G. Marcano, C. Rincón, S.A. López, G.S. Pérez, J.L. Herrera-Pérez, J.G. Mendoza-Alvarez, P. Rodríguez, Raman spectrum of monoclinic semiconductor $Cu_2SnSe_3$, Solid State Commun. 151 (2011) 84.
[10] G. Marcano, C. Rincón, G. Marín, R. Tovar, G. Delgado, Crystal growth and characterization of the cubic semiconductor $Cu_2SnSe_4$, J. Appl. Phys. 92 (2002) 1811.
[11] G. Babu, Y. Kumar, Y. Reddy, V. Raja, Growth and characterization of $Cu_2SnSe_3$ thin films, Mater. Chem. Phys. 96 (2006) 442.
[12] J. Rivet, Contribution l'étude de quelques combinaisons ternaires sulfurées, seleniées ou tellurées du cuivre avec les elements du groupe IV, J. Ann. Chim. 10 (1965) 243.
[13] J.T. Wätjen, J. Engman, M. Edoff, C. P.-B. Solar cells, direct evidence of current blocking by ZnSe in $Cu_2ZnSnSe_4$, Appl. Phys. Lett. 100 (2012) 173510.
[14] A. Redinger, M. Mousel, M.H. Wolter, N. Valle, S. Siebentritt, Influence of S/Se ratio on series resistance and on dominant recombination pathway in $Cu_2ZnSn(SSe)_4$ thin film solar cells, Thin Solid Films 535 (2013) 291.
[15] A. Redinger, R. Djemour, T. Weiss, J. Sendler, L. Gütay, S. Siebentritt, Molecular beam epitaxy of $Cu_2ZnSnSe_4$ thin films grown on GaAs(001), Photovoltaic Specialists Conference (PVSC), IEEE 39th, 2013, p. 0420, http://dx.doi.org/10.1109/PVSC.2013.6744181.
[16] A. Redinger, D.M. Berg, P.J. Dale, S. Siebentritt, The consequences of kesterite equilibria for efficient solar cells, J. Am. Chem. Soc. 133 (2011) 3320.
[17] I. Repins, C. Beall, N. Vora, C.D. Hart, D. Kuciauskas, P. Dippo, B. To, J. Mann, W.-C. Hsu, A. Goodrich, R. Noufi, Co-evaporated $Cu_2ZnSnSe_4$ films and devices, Sol. Energy Mater. Sol. Cells 101 (2012) 154.
[18] D. Regesch, Photoluminescence and Solar Cell Studies of Chalcopyrites; Comparison of Cu-rich vs. Cu-Poor and Polycrystalline vs. Epitaxial Material(Dissertation) University of Luxembourg, 2014.
[19] A.J. Wilkinson, D.J. Dingley, Quantitative deformation studies using electron back scatter patterns, Acta Metall. Mater. 39 (1991) 3047.
[20] S. Karpov, M. Maiorov, Analysis of V-group molecules sticking to III–V compound surfaces, Surf. Sci. 344 (1995) 11.
[21] G. Brammertz, Y. Ren, M. Buffière, S. Mertens, J. Hendrickx, H. Marko, A.E. Zaghi, N. Lenaers, C. Köble, M.M.J. Vleugels, J. Poortmans, Electrical characterization of $Cu_2ZnSnSe_4$ solar cells from selenization of sputtered metal layers, Thin Solid Films 535 (2013) 348.